EFFECT OF INDUCED SEIMICITY OF INDIRECT METEORITE IMPACTS ON THE STABILITY OF LUNAR LAVA TUBES. A. Modiriasari[1*], A. Boener[2], A. K. Theinat[1], A. Bobet[1], H. J. Melosh[2], S. J. Dyke[1,3], J. Ramirez[1], A. Maghareh[1], and D. Gomez[1]. [1,*]Lyles School of Civil Engineering, Purdue University, West Lafayette, IN 47907, amodiria@purdue.edu; [2]Department of Earth, Atmospheric, and Planetary Sciences, Purdue University, West Lafayette, IN 47907; [3]School of Mechanical Engineering, Purdue University, West Lafayette, IN 47907.

Introduction: Lunar lava tubes can potentially serve as secure shelters for future human exploration and permanent extraterrestrial habitats [1-4]. The evidence of the presence of the lava tubes under the surface of the Moon is provided by the images and measurements of the skylights from the LRO and SELENE spacecraft [2, 5-8], LiDAR data from the SELENE [9], and gravity data from the GRAIL mission [10,11]. Based on the GRAIL data, the width of the lunar lava tubes can be as large as 1,000-2,000 m [10,11]. These underground structures can provide immediate protection against hazards such as radiation, temperature fluctuations, and direct meteorite impacts. The stability of the lava tubes under lunar condition has been analyzed using finite element models with different geometric configurations and material properties [12-15]. In this study, first the induced seismicity from indirect meteorite impacts is modeled. Then, the stability of the lava tubes under effects of the induced seismicity is investigated.

Modeling Induced Seismicity: We implemented the shock physics program iSALE-2D [16] in this study to model hypervelocity impacts and then obtain the seismic wave induced by the impact. This program is a development of the earlier SALE hydrocode [17] to include an elasto-plastic material model, fragmentation, equations of state for multiple materials [18,19], a modified strength model [20], and compaction [16,21] and dilatancy models [22] for porous or granular materials. The program models meteorite impacts with high accuracy and provides output for analyzing the effects of the impact [23]. We used tracer data to extract the displacement-time history at determined locations within the code. More specifically, we measured the amplitude and duration of the displacement of various tracers throughout the mesh to obtain the amplitude and frequency content, respectively, of the seismic wave induced by the impact.

All of the simulation meshes had a high-resolution zone of 250 horizontal by 1040 vertical cells, with 40 cells above the surface. So our physical target, in the high-resolution zone, is 250 cells wide by 1000 cells deep. The mesh was extended to 750 horizontal and 500 vertical cells. The extension zone helps assure that no reflections from the boundaries interfere with the analysis. The impact velocity of the meteorite was assumed to be constant at 17 km/s, which is typical for impacts on the Earth or Moon [24]. In the simulations, we assumed that the impactor was made of basalt, the same rock material [18,19] of the lunar basement [25], and the simulations were conducted at 5 Cells-Per-Projectile-Radius (CPPR) resolution. The effects of the regolith cover were not considered in the models and will be part of a future study. The impactor sizes ranged from 0.1 to 5 m in diameter for an impact flux from 4.5×10^{-11} to 7×10^{-18} impacts/m^2/year, respectively [26].

We extracted the motion data from the analyses from beyond any regions that had any significant influence from heating, inelastic material deformation or damage caused by the impact, to get the elastic seismic wave. From impact cratering scaling laws, it can be assumed that the typical impact crater size is ~10 times the radius of the impactor [27]. In early experiments, we determined that the zone of damage caused by an impact is typically ~3-4 times the crater radius. With 5 CPPR in the models, the zone of damage extended horizontally to cells 150-200. This is the reasons why the high-resolution zone was 250 cells wide in the horizontal direction. The tracer field started from cell 100 to the end of the high-resolution zone (cell 250) in the horizontal direction. Therefore, we can ascertain that we analyze the first occurrence of an elastic wave beyond the damage zone. We also want to be able to measure this shockwave down to the depth at which it dissipates to a sufficiently negligible amplitude, so the high resolution zone was 1000 cells deep. The results showed that the damage zone ends at ~15-17 times the impactor size.

Results and Discussion: The displacement-time data in x- and y-directions were obtained for impact diameters of 0.1, 0.5, 1, and 5 m. Only the results of one representative impactor are discussed here. Figures 1a and 1b show the ground motions induced from the 1 m impactor, at a distance of 15.75 m (out of the damage zone) from the impact region and at different depths (z). Note that the negative values in the y-direction are downward.

The results show that: 1) the amplitude of the motions in the y-direction, at each depth, are larger than the corresponding x-displacements; 2) the amplitudes attenuate with depth and approach zero at a depth of ~200 m; 3) the x- and y-displacements approach a steady-state after ~0.05, 0.07 s, respectively.

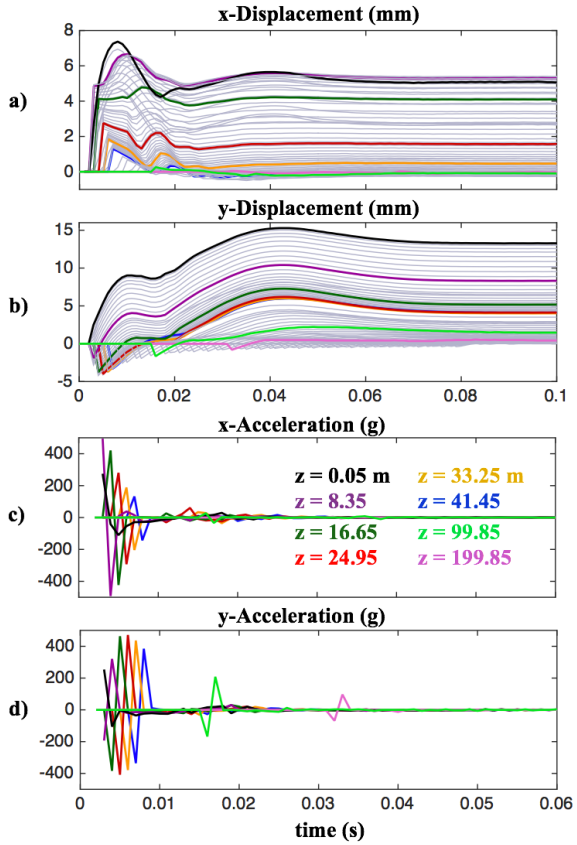

Figure 1. Displacements (a, b) and acceleration (c, d) history obtained from iSALE at 15.75 m distance from the impact point with size of 1 m.

The ground acceleration is shown in Figures 1c and 1d. The results indicate that for shallow depths, up to z~40 m, one large peak ground acceleration, PGA, of ~100g-500g (g is the gravity acceleration on the Earth) is obtained in the x-direction during a short period of time after the impact (before 0.01 s). The PGA decreases to ~20g and 8g at z~100 and 200 m, respectively. As with the displacements, the PGAs in the y-direction is generally larger than in the x-direction.

Future Direction: The structural stability of lava tubes, considering different opening sizes, roof thicknesses, and material properties has been investigated [14]. This was done using 2D plain strain models with the finite element method code ABAQUS© [28]. The material properties of the basaltic rock forming the tubes were estimated based on a Geological Strength Index (GSI) [29] of 50-70 [15]. The results showed that the roof thickness and strength of the basaltic rock (especially tensile strength) significantly affected the stability of the tubes.

In a future study, the effect of induced seismicity from indirect meteorite impacts on the stability of the tubes will be investigated. A 1,000 m width lava tube will be modeled based on the findings from the GRAIL [10,11], inferred results from the collapsed pit data [30], and analytical solutions [15]. The height to width ratio of the lava tube will be taken as 1:3, according to the dimensions of the terrestrial lava tubes [12]. The results of previous studies [15] indicate that for a lava tube width of 1,000 m and GSI of 70, the minimum roof thickness that was required to preserve stability was 100 m [15]. The stability of the tubes with an overburden of 100 m under the effect of induced seismicity will be analyzed. The displacements obtained from the iSALE simulations (Figures 1a and 1b) will be imposed to the lateral boundaries of the model, as shown in Figure 2. The stability of the lava tube will be analyzed by examining the plastic yielding of the rock surrounding the tube, as well as using the convergence criterion [15].

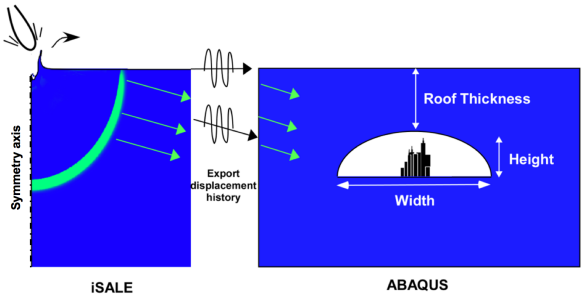

Figure 2. Simulation of the lunar lava tubes stability, in ABAQUS, under effects of induced seismicity of indirect impact, modeled in iSALE.

Acknowledgments: This work is funded by the Purdue Office of the Provost, College of Engineering, Department of Earth, Atmospheric, and Planetary Sciences, Schools of Civil and Mechanical Engineering, and Dubai Future Foundation (DFF). The authors are grateful for the supports.

References: [1] Horz F. (1985) *LPI*, 405-412. [2] Haruyama J. et al. (2012) *Springer*, 139-163. [3] Dyke S.J. et al. (2018) *LPSC*, #2882. [4] Maghareh A. et al. (2018) *LPSC*, #2860. [5] Haruyama J. et al. (2009) *GRL*, *36*, L21206. [6] Haruyama J. et al. (2010) *LPSC*, #1285. [7] Robinson M.S. et al. (2010) *Space Sci.*, *150(1-4)*, 81-124. [8] Robinson M.S. (2012) *Space Sci.*, *69*, 18-27. [9] Haruyama J. et al. (2017) *LPSC*, #1711. [10] Chappaz L. et al. (2017) *GRL*, *44(1)*, 105-112. [11] Sood R. et al. (2017) *Icarus*, *289*, 157-172. [12] Blair D.M., et al. (2017) *Icarus 282*, 47-55. [13] Modiriasari A. et al. (2018) *LPSC*, #2803. [14] Theinat A.K. et al. (2018) *AIAA*. [15] Theinat A.K. et al. (submitted) *Icarus*. [16] Wünnemann K. et al. (2006) *Icarus*, *180(2)*, 514-527. [17] Amsden A.A. et al. (1980) *Int. Nuclear Info. Sys.*, *11(24)*. [18] Melosh H.J. et al. (1992) *JGR*, *97*, 14735-14759. [19] Ivanov B.A. et al. (1997) *Int. J. of Impact Eng.*, *20(1-5)*, 411-430. [20] Collins G.S. et al. (2004) *Meteoritics & Planetary Sci.*, *39(2)*, 217-231. [21] Collins G.S. et al. (2011) *Int. J. of Impact Eng.*, *38(6)*, 434-439. [22] Collins G.S. (2014) *JGR*, *119*, 2600-2619. [23] Guldemeister N. et al. (2017) Icarus, 296, 15-27. [24] Yue Z. et al. (2013) *Nature Geoscience*, *6*, 435. [25] Melosh H.J. (2011) *Cambridge Uni. Press*. [26] Lindsey N.J. (2003) *Int. Lunar Conf.* [27] Melosh H.J. et al. (1989) *Oxford Uni. Press*. [28] ABAQUS, Inc. (2017) *V.6.16 user's manual*. [29] Marinos P. et al. (2000) *Geo. Eng. Conf.* [30] Sauro F. et al. (2018) *LPSC*, #1105.